

## Hurst exponent: A method for characterizing dynamical traps

Daniel Borin<sup>✉</sup>

*São Paulo State University (UNESP), IGCE - Physics Department, 13506-900, Rio Claro, São Paulo, Brazil*



(Received 3 July 2024; accepted 24 October 2024; published 31 December 2024)

Dynamical trapping occurs when the duration of time spent in specific regions of phase space increases, often associated with stickiness around invariant islands during manifold crossings. This paper introduces the Hurst exponent as a tool to characterize the dynamics of a typical quasi-integrable Hamiltonian system with coexisting regular and chaotic regions. Beyond detecting chaotic orbits and sticky regions, applying a finite-time analysis reveals a multimodal distribution of the finite-time Hurst exponent, where each mode corresponds to motion around islands of different hierarchical levels. The advantage of the Hurst exponent method over other standard techniques lies in its ability to quickly indicate chaotic dynamical structures. It effectively distinguishes between quasiperiodic and chaotic orbits temporarily trapped in sticky domains using very short trajectories. Additionally, since it operates based on time series data, it facilitates the exploration of trapping effects in dynamic systems that lack well-defined laws, a common scenario in natural dynamics.

DOI: [10.1103/PhysRevE.110.064227](https://doi.org/10.1103/PhysRevE.110.064227)

### I. INTRODUCTION

Hamiltonian systems represent a category of dynamical systems that elucidate the dynamic behavior of particles in motion, relying on the principle of energy conservation. Within this group, a distinction arises between integrable and nonintegrable Hamiltonian systems. In integrable Hamiltonian systems, the motion of particles follows regular and discernible patterns. Conversely, nonintegrable Hamiltonian systems present a more intricate and unpredictable nature, where the phase space exhibits a complex combination of regularity and chaos, featuring Kolmogorov-Arnold-Moser (KAM) islands, invariant tori, spanning curves, and chaotic seas [1]. Due to the existence of islands scattered throughout the chaotic sea, the sea forms a fat fractal [2], making it hard to say exactly where one island ends and another begins. Larger islands are surrounded by smaller ones, and those smaller ones are in turn surrounded by even smaller islands. This pattern repeats at smaller and smaller scales, creating an endless hierarchy of islands within islands. [3] These characteristics introduce features such as dynamical traps, which affect the diffusion process [4], leading to intriguing properties in the dynamics.

In a general sense, the dynamical trap is a domain in phase space where a particle (or its trajectory) can spend arbitrarily long finite time, performing almost regular dynamics, called a flight, even though the entire trajectory is random in any appropriate sense [5]. In a chaos scenario, there are the dynamical traps named stickiness [6–12], which emerge when orbits, initially influenced by chaotic dynamics, exhibit a prolonged interaction with specific regions characterized by regular behavior, such that these trajectories become temporarily “stuck” or trapped to particular structures within the

phase space for a time that may be, eventually, long. This phenomenon affects global properties of the system, such as the decay of correlations [8,13,14] and transport [9]. Before escaping, the orbits are confined within a region bounded by cantori [15], a Cantor set formed from the remnants of the destroyed KAM tori. This structure serves as a partial barrier to the transport in phase space and can be trapped in the region cantori enclosed. Once inside a cantorus, chaotic orbits can cross into an inner cantorus. This process can continue to infinitely small scales within the hierarchical structure of islands around islands [16].

A way to quantify these trap effects is the finite-time Lyapunov exponent (FTLE) [17,18] that measures the exponential rates of principal divergences of the initially neighboring trajectories during finite-time intervals. However, computing requires a well-defined law that describes the orbit, which is unavailable in some natural dynamics. Moreover, these exponents might not be the most effective method for detecting stickiness. Once an orbit is trapped, the largest Lyapunov exponent decreases, slowing down its convergence—it takes longer to reach its asymptotic (infinite-time) value.

Recently, a new method has been proposed to detect chaotic orbits by calculating the Shannon entropy of the recurrence time [19–21]. It has proven to be a better option for distinguishing between regular and chaotic orbits than the Lyapunov exponents. However, it has only applied in situations where the Slater theorem [22,23] is valid.

This paper presents a measure to identify regular, chaotic, and sticky regions: the Hurst exponent, which is essentially a measure of the long-term memory of time series. Using the Hurst exponent, it is possible to distinctly identify both the regular regions and the transitions to chaotic motion as a system parameter varies. Additionally, computing the finite-time Hurst exponent (FTH) distribution reveals a multimodal pattern, where each peak corresponds to a distinct hierarchical level within the islands-around-islands structure.

\*Contact author: d.borin@hotmail.com

This paper is structured as follows: In Sec. II, the Hurst exponent is introduced. In Sec. III, the standard map is presented, followed by a brief discussion of the properties of two-dimensional quasiintegrable Hamiltonian systems. In Sec. IV, the Hurst exponent is applied to detect and characterize sticky orbits in this system. Moreover, a finite-time analysis is conducted, leading to a distribution of the finite-time Hurst exponent related to the motion around islands of different hierarchical levels. Additionally, the methodology is also applied to the bouncer and kicked Harper maps in Sec. V to further validate the approach. Finally, Sec. VI presents the concluding remarks.

## II. HURST EXPONENT

The Hurst exponent, proposed by Hurst [24] in 1951 to statistically model the cycle of Nile floods, is essentially a measure of long-term memory of time series. The main advantage of the method is that it can be calculated with few assumptions about the underlying system, given its broad applicability for time series analysis in the finance market [25–28], in electrocardiogram data, providing auxiliary features for the classification of heart disease data [29], and in some cases can be experimentally measured [30].

Essentially, the Hurst exponent is confined to the range between zero and one, and categorized into three distinct classes:

- (1)  $H = 1/2$  indicates random series (uncorrelated process);
- (2)  $H > 1/2$  indicates a persistent (long-term memory, correlated) process;
- (3)  $H < 1/2$  indicates an antipersistent (short-term memory, anticorrelated) process.

A wide array of computational algorithms are available [31] for estimating the Hurst exponent, such as detrended fluctuation analysis (DFA) [32], detrended moving average (DMA) [33], periodogram method (PM) [34], etc. Among them, the rescaled range analysis (R/S analysis) stands out as the oldest and most renowned [24], popularized by Mandelbrot's works [35,36]. He found [37] that the fractal dimension  $D$  and the Hurst exponent  $H$  are related by the expression  $D = 2 - H$ . This relation establishes the connection between the statistical properties of time series and their underlying fractal characteristics.

In this approach, given a time series  $X = X_1, X_2, \dots, X_L$  of full length  $L$ , then

- (i) Divide the time series into  $K$  subseries  $P_{k,\ell}$  of length  $\ell$ , such that the number of chunks  $K$  satisfies  $K = L/\ell$ . Each subseries is denoted by  $P_{k,\ell} = [X_{(k-1)\ell+1}, X_{k\ell}]$  with  $k = 1, 2, \dots, K$ .
- (ii) For each subseries  $k = 1, 2, \dots, K$ , calculate the mean  $\mu_{k,\ell}$ , standard deviation  $S_{k,\ell}$ , and the deviations from the mean:

$$D_{i,k,\ell} = P_{i,k,\ell} - \mu_{k,\ell},$$

where  $i$  denotes the elements.

- (iii) Compute cumulative sums of deviations

$$Z_{i,k,\ell} = \sum_{j=1}^i D_{j,k,\ell}$$

for  $i = 1, 2, \dots, \ell$ .

- (iv) Calculate the range of the cumulative deviation  $R_m$  of each subseries  $Z_k$ ,

$$R_{k,\ell} = \max_{1 \leq i \leq \ell} (Z_{i,k,\ell}) - \min_{1 \leq i \leq \ell} (Z_{i,k,\ell}).$$

- (v) Calculate the mean of the rescaled ranges,

$$(R/S)_\ell = \left\langle \frac{R_{k,\ell}}{S_{k,\ell}} \right\rangle_k = \frac{1}{K} \sum_{k=1}^K \frac{R_{k,\ell}}{S_{k,\ell}}.$$

- (vi) Repeat the process considering another value for  $\ell$ , that is, dividing the time series into another number of subseries.

- (vii) Estimate the Hurst exponent  $H$  by assuming a power-law relationship

$$(R/S)_\ell = C\ell^H$$

and use regression analysis to find  $H$ .

Note that a unique Hurst value is associated with the size  $L$  of a time series. Therefore, the notation  $H(L)$  will be utilized throughout the text.

In the case of a bidimensional temporal series  $W = (X_1, Y_1), (X_2, Y_2), \dots, (X_L, Y_L)$ , it is necessary to adapt the R/S analysis. The time series is divided into  $K$  chunks as before; however, each subperiod is now defined by  $P_k = (X_{(k-1)\ell+1}, Y_{(k-1)\ell+1}, \dots, X_{k\ell}, Y_{k\ell})$ . The method is executed in the same manner, with the length of each subseries now being  $2\ell$ .

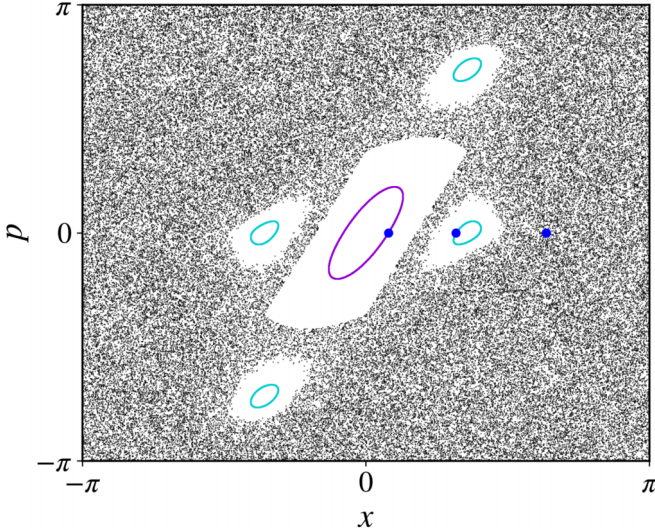
In the Appendix, a scheme of the method utilized in this paper is presented, designed to enhance clarity and intuitive understanding.

## III. STANDARD MAP

It is appropriate to present results employing a widely recognized general model with extensive applications, the Chirikov standard mapping, as defined by Chirikov [38],

$$\begin{aligned} p_{n+1} &= p_n - K \sin(x_n) \quad \text{mod } 2\pi, \\ x_{n+1} &= x_n + p_{n+1} \quad \text{mod } 2\pi, \end{aligned} \quad (1)$$

where  $K$  is the nonlinearity parameter, and  $x_n$ ,  $p_n$  are the position and momentum at discrete times  $n \in \mathbb{N}$ . For  $K = 0$ , the dynamics are regular, and the system is integrable, with every orbit lying on a rotationally invariant torus. As  $K$  increases, some irrational tori remain invariant while resonant tori are destroyed, as described by the KAM theorem. This progression allows for the possibility of observing chaotic behavior under appropriate initial conditions. Specifically, when  $K$  reaches the critical value  $K_c \approx 0.97163540631$  [39], the last invariant rotational torus is destroyed. For  $K > K_c$ , the system exhibits large chaotic orbits, indicative of a global stochastic scenario (global chaos) [40]. Moreover, the system displays sticky behavior, in addition to strictly regular and chaotic regions [41].

FIG. 1. Phase space of the standard map for  $K = 2.5$ .

In the scenario where the phase space contains quasiperiodic islands mixed with regions of chaotic orbits, one would expect to observe stickiness. Figure 1 illustrates this situation considering  $K = 2.5$ , where each orbit was iterated for  $N = 10^5$ . The quasiperiodic orbits are illustrated by the colors purple and cyan with initial conditions  $(x_0, y_0) = (0.25, 0)$  and  $(x_0, y_0) = (1, 0)$ , respectively, while the chaotic orbit is illustrated in black generated by the initial condition  $(x_0, y_0) = (2, 0)$ . The blue points in the phase space denote the initial conditions used to generate the orbits.

This configuration will be utilized in the paper to investigate the occurrence of stickiness. The next section will characterize this phenomenon using the Hurst exponent.

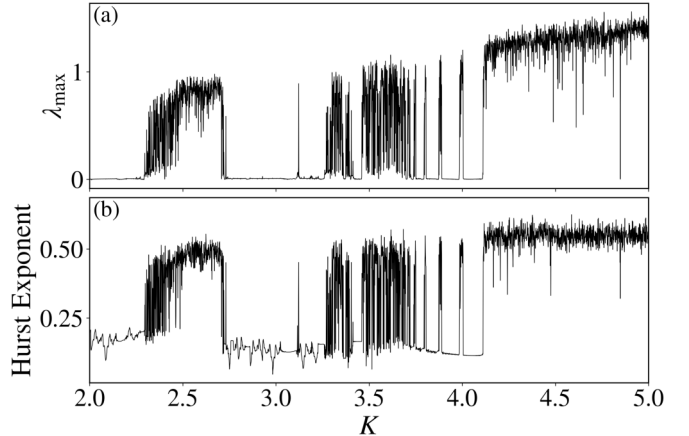
#### IV. INFLUENCE OF TRAPS IN THE DYNAMICS OF THE STANDARD MAP

The concept of stickiness is typically characterized using Lyapunov exponents [42]. However, these exponents have certain limitations: their computation relies on a well-defined law describing the orbit, which is often unavailable in natural dynamics. Moreover, once an orbit becomes trapped, the largest Lyapunov exponent decreases, slowing its convergence toward its asymptotic (infinite-time) value. In this section, we evaluate the Hurst Exponent for the standard map and demonstrate its utility in characterizing the system's dynamics.

The most traditional and widely recognized method for characterizing the dynamics of a system is through the evaluation of Lyapunov exponents [43–45], which quantify the average rate of expansion or contraction for a small volume of initial conditions. The Lyapunov exponents are defined as [46]

$$\lambda_j = \lim_{n \rightarrow \infty} \frac{1}{n} \ln |\Lambda_j^{(n)}|, \quad j = 1, 2, \dots, d,$$

where  $j$  are the eigenvalues of the matrix  $M = \prod_{i=1}^n J_i$  with  $J_i$  being the Jacobian matrix evaluated over the orbit, and  $d$  is the dimension of the system. For our two-dimensional system ( $d = 2$ ), there are two exponents,  $\lambda_1$  and  $\lambda_2$ , satisfying

FIG. 2. (a) The maximum Lyapunov exponent  $\lambda_{\max}$  and (b) the Hurst exponent  $H$  for the standard map, plotted as functions of the parameter  $K$  with the initial condition  $(x_0, p_0) = (0.0, 1.3)$ .

$\lambda_1 \geq \lambda_2$ . The maximum Lyapunov exponent,  $\lambda_{\max} := \lambda_1$ , is used to characterize the system's dynamics: periodic regimes are indicated by a negative  $\lambda_{\max}$ , while chaotic dynamics are identified by a positive  $\lambda_{\max}$ . When an orbit is captured by a dynamical trap for a period of time, certain properties are affected, particularly the maximum Lyapunov exponent,  $\lambda_{\max}$ . Although both chaotic and sticky orbits exhibit positive values of  $\lambda_{\max}$ , the value for a sticky orbit is lower than that of a chaotic orbit. For a quasiperiodic orbit,  $\lambda_{\max}$  is small but not exactly zero, due to the finite iteration time,  $N$ .

First, let's compare the maximum Lyapunov exponent with the Hurst exponent. In Fig. 2(a), this comparison is shown, where the values of  $\lambda_{\max}$  and  $H$  of the standard map are plotted as functions of the nonlinearity parameter  $K$ , with a fixed initial condition  $(x_0, p_0) = (0.0, 1.3)$  iterated for  $N = 2^{10}$ . This plot reveals windows of regularity characterized by  $\lambda_{\max}$  being zero and  $H$  taking on low values. Although the Lyapunov exponent approaches zero more rapidly near the elliptic point [47], it alone cannot differentiate between periodic and quasiperiodic orbits in bidimensional Hamiltonian systems. Note that for several values of the parameters  $K$ , the Hurst exponent  $H$  is close to zero, indicating that at these points, the initial condition  $(x_0, p_0) = (0.0, 1.3)$  is very close to a periodic orbit, as illustrated in Fig. 2(b).

Directing our attention to the phase space, Fig. 3 displays the values of  $\lambda_{\max}$  and  $H$  for a grid of initial conditions uniformly distributed in the phase space  $(x, p)$  with  $K = 2.5$ , where the initial condition was iterated for  $N = 2^{10}$ . It includes a zoom into one of the four-period satellite islands, as well as exploration in the parameter space. One can observe that the Hurst exponent  $H$  captures the characteristics exhibited by the Lyapunov exponent and more. In the chaotic sea, where  $\lambda_{\max}$  is large,  $H$  is also large. Conversely, inside the islands, where  $\lambda_{\max}$  is low, the  $H$  is correspondingly low. Additionally, in regions where the rotation number of an orbit approaches a rational value,  $H$  is smaller [indicated by the transition from purple to black in 3(d)], characterizing trapped regions [48,49]. Moreover, Fig. 3(f) clearly shows transitions from regular to chaotic behavior, as well as bifurcations as  $K$  changes. Finally, it is observed from Figs. 3(g)–3(l) that all

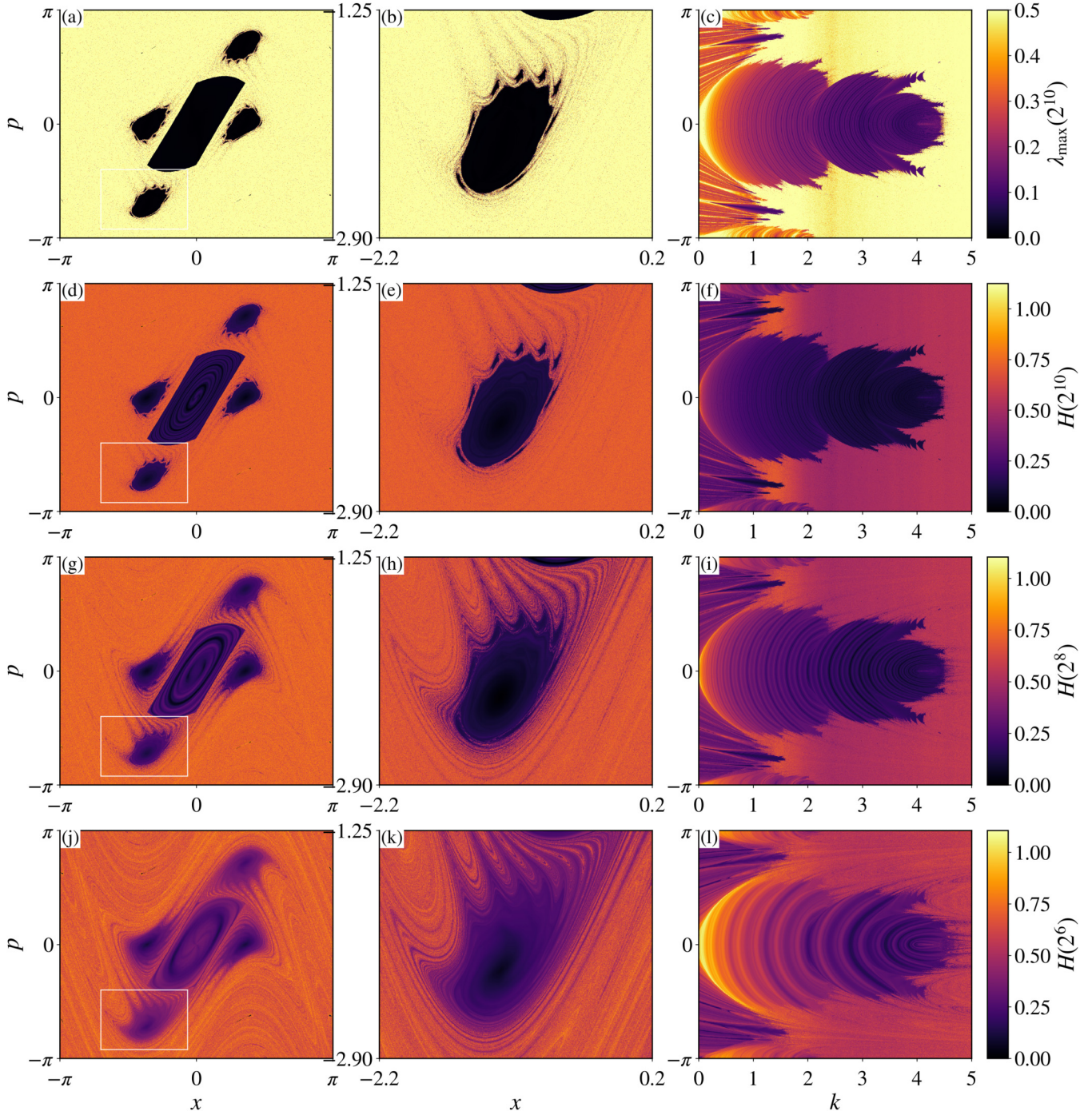


FIG. 3. (a)–(c) The maximum Lyapunov exponent  $\lambda_{\max}$  and (d)–(f) the Hurst Exponent  $H$  for the standard map, evaluated on a  $2^{10} \times 2^{10}$  grid of uniformly distributed points in the phase space  $(x, p)$ , with  $K = 2.5$ . Subfigures (a), (b), (d), (e), (g), (h), (j), and (k) depict results in the phase space, while (c), (f), (i), and (l) show results in the parameter space  $(K, p)$ , with  $x_0 = 0$ . (b), (e), (h), and (k) provide magnified views of the regions delineated by the white rectangles in (a), (d), (g), and (j), respectively.

the conclusions drawn in the preceding analysis remain valid when reducing the number of interactions, i.e., considering a shorter time series. In these scenarios, it is evident that the regions with low values of  $H$  increase, and the trajectories of orbits passing through the four principal islands continue to be consistent. Finally, the results stay robust for different values of the nonlinear parameter, as shown in Fig. 4.

After these analyses, the results demonstrate that the Hurst exponent is an excellent measure for distinguishing between

periodicity, weak chaos, and strong chaos. Additionally, it is a fast indicator for chaotic dynamical structures, obtaining robust results with the Hurst exponent using only a short time series of  $2^6$  data points, as illustrated in Figs. 3(j)–3(l).

A way to quantify dynamical traps is the finite time Lyapunov exponent (FTLE), which can also characterize stickiness in high-dimensional Hamiltonian systems [42]. Szezech *et al.* [18] demonstrated that in phase spaces with stickiness regions, the distribution of finite-time Lyapunov ex-

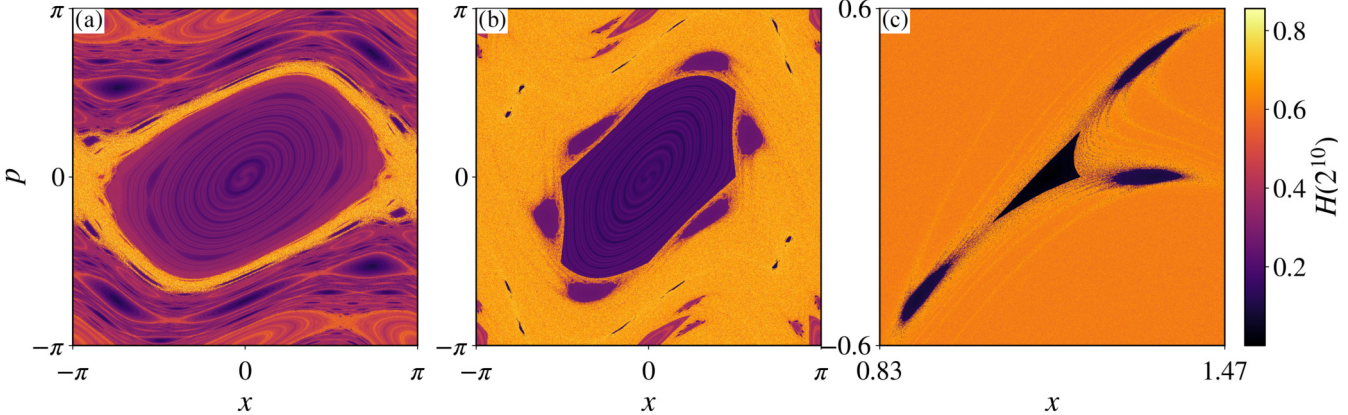


FIG. 4. The Hurst exponent  $H$  for the standard map, evaluated on a  $2^{10} \times 2^{10}$  grid of uniformly distributed points in the phase space  $(x, p)$  considering the nonlinear parameter as (a)  $K = 0.9$ , (b)  $K = 1.6$ , and (c)  $K = 6.908745$ .

ponents is bimodal. However, Harle and Feudel [50] suggest that the minor peak in this distribution consists of multiple peaks, and Sales *et al.* [19] verified this hypothesis using recurrence time entropy.

Examining any single chaotic orbit over a long duration reveals that the particle, while essentially confined within the chaotic sea, passes near periodic regions and may become trapped for a significant period before eventually escaping to the chaotic sea. Therefore, it is essential to conduct a finite-time analysis to accurately detect transitions between different regimes in the orbit's dynamics.

To perform this analysis, an initial condition  $(x_0, p_0)$  is chosen from within the chaotic sea. This initial condition is iteratively evolved to generate a time series of length  $N$ . Subsequently, this series is segmented into windows of size  $T$ , and the Hurst exponent  $H$  is computed for each window, denoted as  $FTH_T(N)$ . An alternative approach involves evaluating a single chaotic orbit over a time interval  $T$ , calculating  $H$ , and repeating this process by initializing a new orbit at the end of each iteration, performing  $M = N/T$  times. Additionally, the probability distribution of the Hurst exponent over finite-time intervals,  $P(FTH_T(N))$ , is defined by constructing a frequency histogram of  $FTH_T(N)$ . In Figs. 5(a)–5(c), this distribution is depicted for  $N = 2^{30}$  with the initial condition  $(x_0, p_0) = (-3, 0)$  and  $K = 2, 5$ .

Such distributions can be understood as follows: when the orbit is in the chaotic region, the distribution tends to exhibit values near the larger maximum. However, when the trajectory remains trapped for some time, small values for the Hurst exponent are registered. When the orbit is confined near an island, it may enter a deeper level within the hierarchical structure, resulting in a multimodal distribution. Therefore, the infinite hierarchical islands-around-islands structure is responsible for the multiple small peaks in the distribution.

A critical consideration when employing finite-time Hurst exponents (FTH) is the potential time dependence of the results. Specifically, with longer observation periods and different time windows, would the distribution of FTH vary? To investigate this, Figs. 5(a)–5(c) illustrate the FTH distribution for three distinct time windows, and Fig. 6 shows results across three different trajectory lengths  $N$  at a  $K = 2.5$  value. Remarkably, the findings demonstrate insensitivity to the total

duration of system iteration. This observation is due to the phenomenon in Hamiltonian systems where longer trajectories increase the likelihood of encountering trapping regions. Moreover, greater trajectory lengths enhance the probability of encountering trap regions with prolonged times. Consequently, finite-time Hurst exponents serve as a valuable metric for assessing the significance of trap regions in system dynamics, offering a robust statistical representation across the entire phase space.

To identify the regions corresponding to distribution peaks, phase space positions are plotted in Fig. 5 based on the Hurst exponent values, considering distinct time window sizes of  $2^6$ ,  $2^7$ , and  $2^8$ . Each peak of the distribution is represented by a color in the phase space, indicating different hierarchical levels within the structure, discernible through Hurst analysis. Figures 5(d)–5(f) illustrate the manifolds where nontrapped orbits exit sticky regions [51], highlighting nonhyperbolicity, which can restrict chaotic orbits from accessing certain domains due to stable and unstable manifold tangencies [52]. In addition, Figs. 5(g)–5(i) depicts hierarchical levels around the four-period island, with all island chains being very well evident even when changing the time window size.

## V. APPLICATIONS IN OTHER MODELS

To validate the use of the Hurst exponent in characterizing dynamical traps in Hamiltonian systems, this formalism is applied to two additional systems: the bouncer model and the kicked Harper map.

### A. Bouncer model

The bouncer model describes a simple dynamical system where a classical particle, like a ball, moves vertically under the influence of a constant gravitational field and repeatedly bounces on a periodically oscillating surface. The origins of this model trace back to Pustyl'nikov's work [53–55], where he rigorously demonstrated that certain parameter choices can lead to an unbounded increase in the particle's velocity, a phenomenon known as "Fermi acceleration" [56]. The system's dynamics depend on the nature of the collisions, which can be categorized as (i) multiple collisions, where

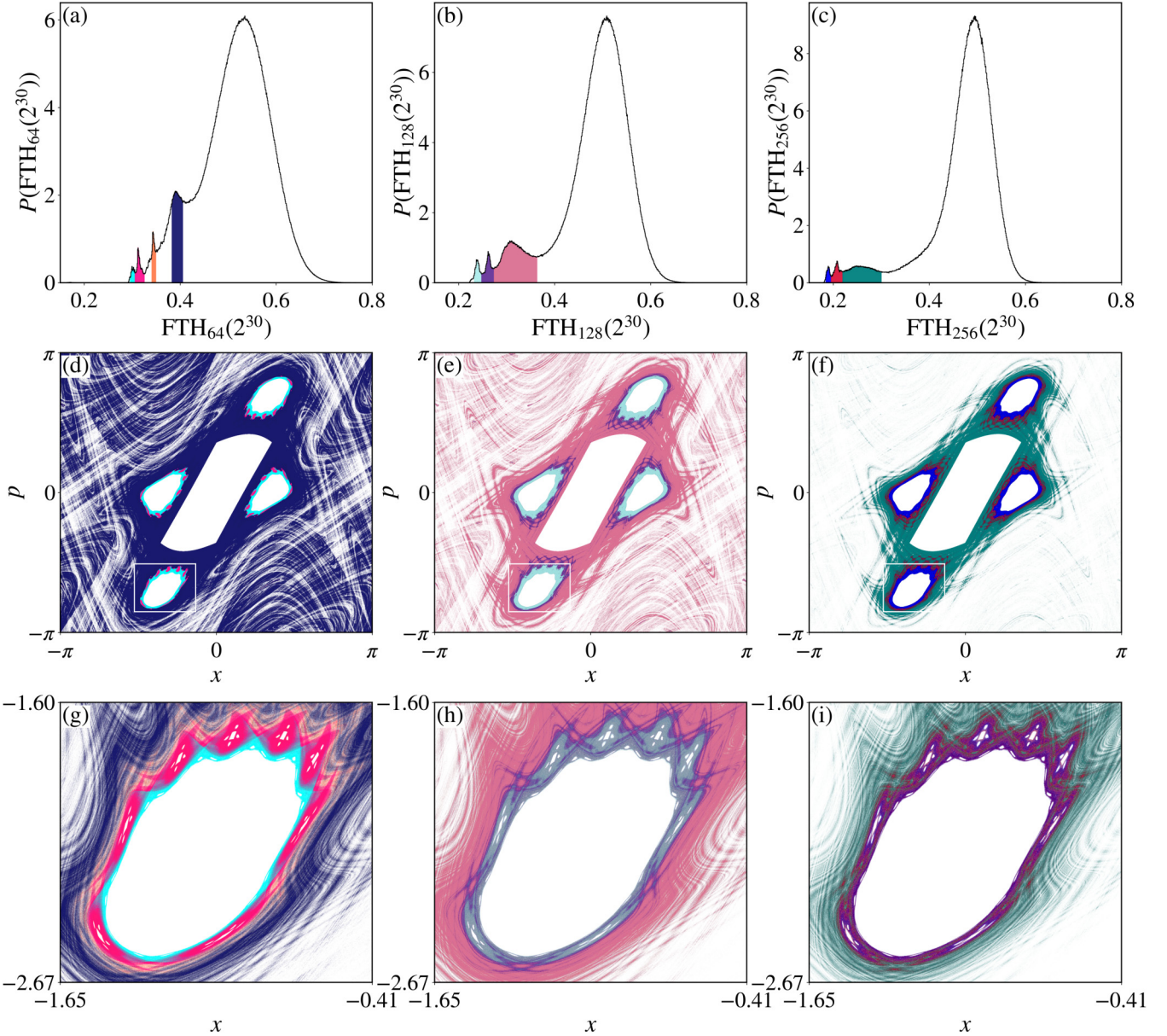


FIG. 5. The finite-time Hurst exponent distribution for a single chaotic orbit, with  $N = 2^{30}$ ,  $K = 2.5$ , and  $(x_0, y_0) = (-3, 0)$  and time window (a)  $T = 2^6$ , (b)  $2^7$ , and (c)  $T = 2^8$ ; (d)–(f) the phase space points that generate the minor peaks in (a)–(c), respectively; and (g)–(i) is a magnification of one of the four-period satellite islands of (d)–(f), respectively, indicated by the white rectangles. The colors in (d)–(i) match the filling colors of the distribution in (a)–(c).

the particle repeatedly interacts with the moving wall before exiting the collision zone (defined as the region where the wall moves), or (ii) a single collision, where the particle leaves the collision zone after impact. Both scenarios typically require solving transcendental equations. To avoid the computationally expensive process of solving these equations—especially in the past when computing power was limited (see [57] for historical context)—a simplified version was introduced. In this approximation, the wall is assumed to be fixed, eliminating the need to calculate the time between collisions using transcendental equations. Instead, at each collision, the particle undergoes an exchange of energy and momentum as if the wall were moving. This approach preserves most of the properties observed in the full version of the model

while simplifying the computations by avoiding transcendental equations. In this static wall approximation, the position of the wall is no longer considered, and the canonical variables become velocity and time, since the phase space has a repeating structure in  $\pi$  in the velocity axis [58], will be considered mod( $\pi$ ) for velocity. Thus, under these considerations, the mapping that describes the dynamics of the model can be expressed as [58–60]

$$\begin{aligned} V_{n+1} &= |V_n - 2\epsilon \sin(\phi_{n+1})| \quad \text{mod } \pi, \\ \phi_{n+1} &= \phi_n + 2V_n \quad \text{mod } 2\pi, \end{aligned} \quad (2)$$

where a set of dimensionless variables is introduced:  $\epsilon = \varepsilon\omega^2/g$ ,  $V_n = v_n\omega/g$ , and  $\phi = \omega t$ . In this context,  $v_n$  is the particle's velocity,  $g$  is the gravitational constant, and  $\varepsilon$  and

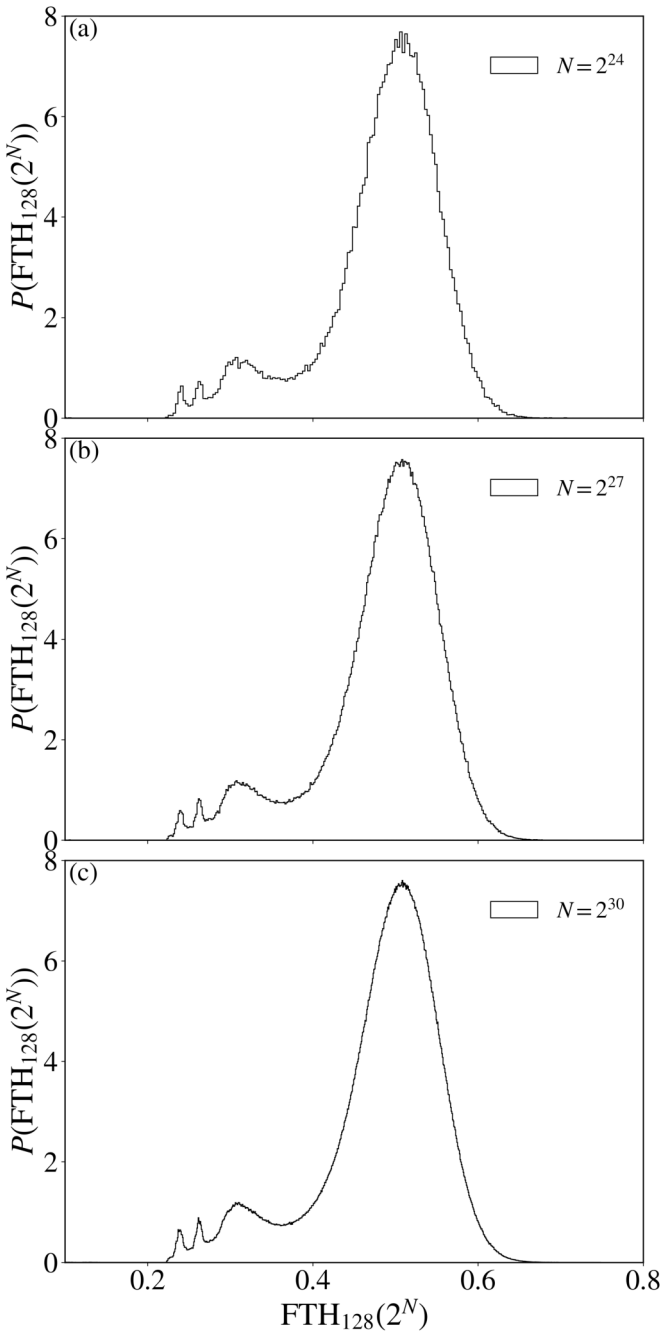


FIG. 6. Behavior of the finite-time Hurst exponent for different sizes of time series.

$\omega$  are the amplitude and frequency of the wall's oscillation, respectively. The modulus function is used to prevent the particle from moving beyond the wall.

Applying the methodology based on the Hurst exponent to detect dynamical traps, in Fig. 7(a), the calculation of  $H$  for a grid of initial conditions uniformly distributed in the phase space  $(x, p)$  with  $K = 0.4$  is performed, where the initial conditions were iterated for  $N = 2^{10}$ . One can see that in the region dominated by the chaotic sea,  $H$  assume high values. Conversely, inside the islands, the values of  $H$  becomes low. Performing a finite time analysis in order to quantify this phenomenon, it examines a single chaotic orbit

with initial condition  $(1, 1)$  of size  $N = 2^{30}$  and it calculates the  $FTH_T(N)$ , considering time window size of 128.

Applying the methodology based on the Hurst exponent to detect dynamical traps, Fig. 7(a) shows the values of  $H$  for a grid of initial conditions uniformly distributed in the phase space  $(x, p)$  with  $\epsilon = 0.4$ , where the initial conditions were iterated for  $N = 2^{10}$ . It is observed that in regions dominated by chaotic behavior,  $H$  assumes high values, while within the islands,  $H$  takes on lower values. To further quantify this phenomenon, a finite-time analysis is conducted by examining a single chaotic orbit with the initial condition  $(x_0, y_0) = (1, 1)$  over a large number of interaction  $N = 2^{30}$  iterations, and the finite-time Hurst exponent  $FTH_T(N)$  is calculated using a time window size of 128. Figure 7(b) displays the probability distribution  $P(FTH_{128}(2^{30}))$  for  $\epsilon = 0.4$ . Livoratti *et al.* [58] reported that for this value of  $\epsilon$ , the distribution of the finite-time Lyapunov exponent is bimodal. However, Fig. 7(b) shows that the minor peak actually consists of multiple peaks. In Fig. 7(c), these multiple peaks in the distribution are mapped to corresponding regions in the phase space, with each peak represented by a different color. The results indicate that the distinct peaks in the distribution correspond to different hierarchical structures within the phase space, as identified through the Hurst analysis.

## B. Kicked Harper map

The Harper model, introduced in 1955 [61], describes the motion of crystal electrons in a two-dimensional lattice under a magnetic field, specifically the effect of a uniform magnetic field on a conduction-band metal, where a tight-binding approximation for symmetric cubic crystals is assumed. The semiclassical interpretation of the Harper model leads to an effective one-dimensional Hamiltonian, expressed as [62]

$$H_{\text{HM}}(q, p, t) = -V_2 \cos(2\pi p) - V_1 \cos(2\pi q). \quad (3)$$

The properties of the Harper Hamiltonian, as described by Eq. (3), have inspired studies on the transition from regular to chaotic behavior, particularly through a variant known as the kicked Harper model. This generalized version of the Harper model is expressed as [63,64]

$$H_{\text{KHM}}(q, p, t) = -V_2 \cos(2\pi p) - V_1 \cos(2\pi q)K(t) \quad (4)$$

with

$$K(t) = \tau \sum \delta(t - n\tau),$$

where  $m$  is an integer,  $\tau$  is the period between the kicks, and  $V_1$  and  $V_2$  are constants.

In the limit  $\tau \rightarrow 0$ , the model (4) reduces to the continuous time evolution of the Harper Hamiltonian  $H_{\text{HM}}$ , given by Eq. (3), which is integrable from a dynamical perspective, but for nonzero values, it displays more complex dynamics. The classical map resulting from integrating the equations of motion between successive kicks is given by [65–67]

$$\begin{aligned} p_{n+1} &= p_n - \gamma_1 \sin(2\pi q_n) \pmod{1}, \\ q_{n+1} &= q_n + \gamma_2 \sin(2\pi p_{n+1}) \pmod{1}, \end{aligned} \quad (5)$$

where  $\gamma_i = 2\pi V_i \tau$ . The motion is confined to a toroidal phase space  $(q, p) \in [0, 1] \times [0, 1]$ . In addition, this map can also be derived from the Hamiltonian of the kicked oscillator model,

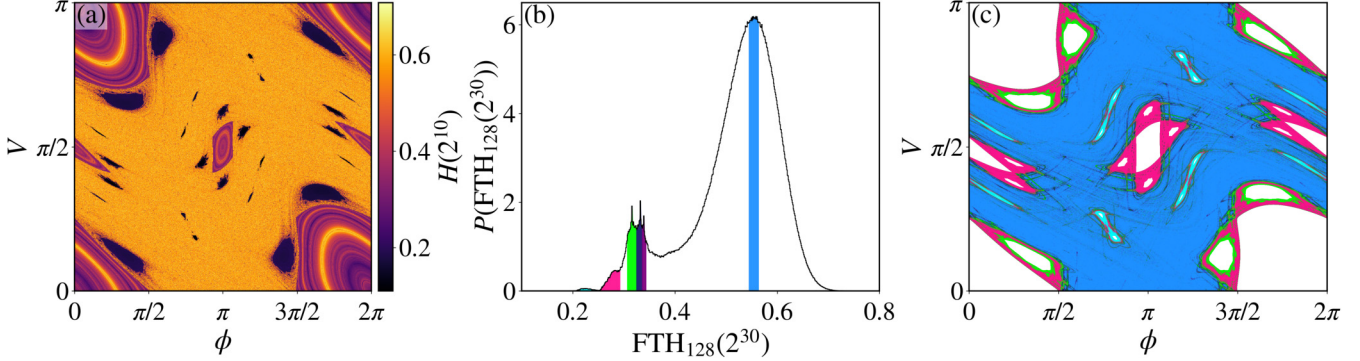


FIG. 7. Application of the methodology to the bouncer map (2) with  $\epsilon = 0.4$ . In (a), the Hurst exponent is calculated on a  $2^{10} \times 2^{10}$  grid of uniformly distributed points in the phase space  $(x, p)$ , considering an orbit of length  $2^{10}$ . In (b), the finite-time Hurst exponent distribution for a single chaotic orbit is shown, with  $N = 2^{30}$ , initial conditions  $(x_0, y_0) = (1, 1)$ , and a time window  $T = 2^7$ . In (c), the phase space points corresponding to the colored peaks in the distribution from (b) are depicted.

which is a linear' oscillator excited by periodic  $\delta$ -like impulses [68,69]:

$$H_{\text{KOM}}(u, v, t) = \frac{1}{2}(u^2 + v^2) - K \cos(q)\tau \sum \delta(t - n\tau), \quad (6)$$

where  $u$  and  $v$  represent the dimensionless momentum and position,  $\alpha$  is the oscillator's rotation angle between kicks,  $t$  is the dimensionless time, and  $K$  is the kick strength. The differential equation for this motion (which is equivalent to that of a particle moving in a constant magnetic field and subjected to a wave packet traveling perpendicularly to it), can be represented in mapping form [70,71]:

$$u_{n+1} = (u_n + K \sin v_n) \cos \alpha + v_n \sin \alpha, \quad (7)$$

$$v_{n+1} = -(u_n + K \sin v_n) \sin \alpha + v_n \cos \alpha. \quad (8)$$

Under the resonance condition [72]  $\alpha = \frac{2\pi}{q}$ , the particle experiences  $q$  kicks over a full oscillation period. For  $q = 4$  (resulting in four kicks per oscillation period), iterating the map four times and retaining only the lowest-order terms in  $K$ , we obtain an alternative form of the "kicked Harper map"

[73]:

$$\begin{aligned} v_{n+1} &= v_n - 2K \sin(u_n), \\ u_{n+1} &= u_n + 2K \sin(v_{n+1}). \end{aligned} \quad (9)$$

Note that Eq. (9) is equivalent to Eq. (5) when  $\gamma_1 = \gamma_2 \equiv 2K$ . Thus, the discussion in this paper will consider the kicked Harper map given by (5) restricted to the special case where  $\gamma_1 = \gamma_2 = \gamma$ .

This model has numerous applications, including the study of charged particles interacting with an electrostatic wave packet in a transverse uniform magnetic field [68,74,75], the motion of electrons in a two-dimensional periodic potential with a uniform magnetic field [64,76], and the steady-state dynamics of ideal incompressible fluids [77,78].

Performing a Hurst exponent analysis to detect dynamical traps, Fig. 8(a) illustrates the values of  $H$  across a grid of initial conditions uniformly distributed within the phase space  $(x, p)$  for  $\gamma = 0.25$ . The initial conditions were iterated up to  $N = 2^{10}$ . It is observed that  $H$  exhibits high values in chaotic regions and lower values within the islands. To better understand this behavior, a finite-time analysis was performed on a single chaotic trajectory with the initial condition  $(x_0, y_0) = (0.5, 0.1)$ , using  $N = 2^{30}$  iterations and a time window size

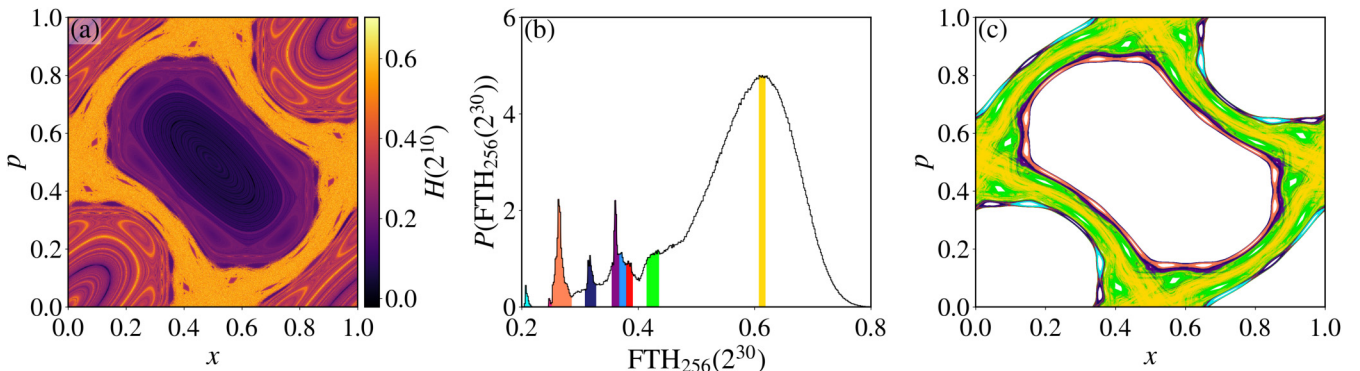


FIG. 8. Analysis of the stickiness in the kicked Harper map (5) with  $\gamma = 0.25$ . In (a), the Hurst exponent is evaluated on a  $2^{10} \times 2^{10}$  grid of uniformly distributed points within the phase space  $(x, p)$ , using an orbit of length  $2^{10}$ . In (b), the distribution of the finite-time Hurst exponent for a single chaotic trajectory is shown, with  $N = 2^{30}$ , initial conditions  $(x_0, y_0) = (0.5, 0.1)$ , and a time window  $T = 2^8$ . In (c), the phase space points responsible for the colored peaks in the distribution from (b) are depicted.

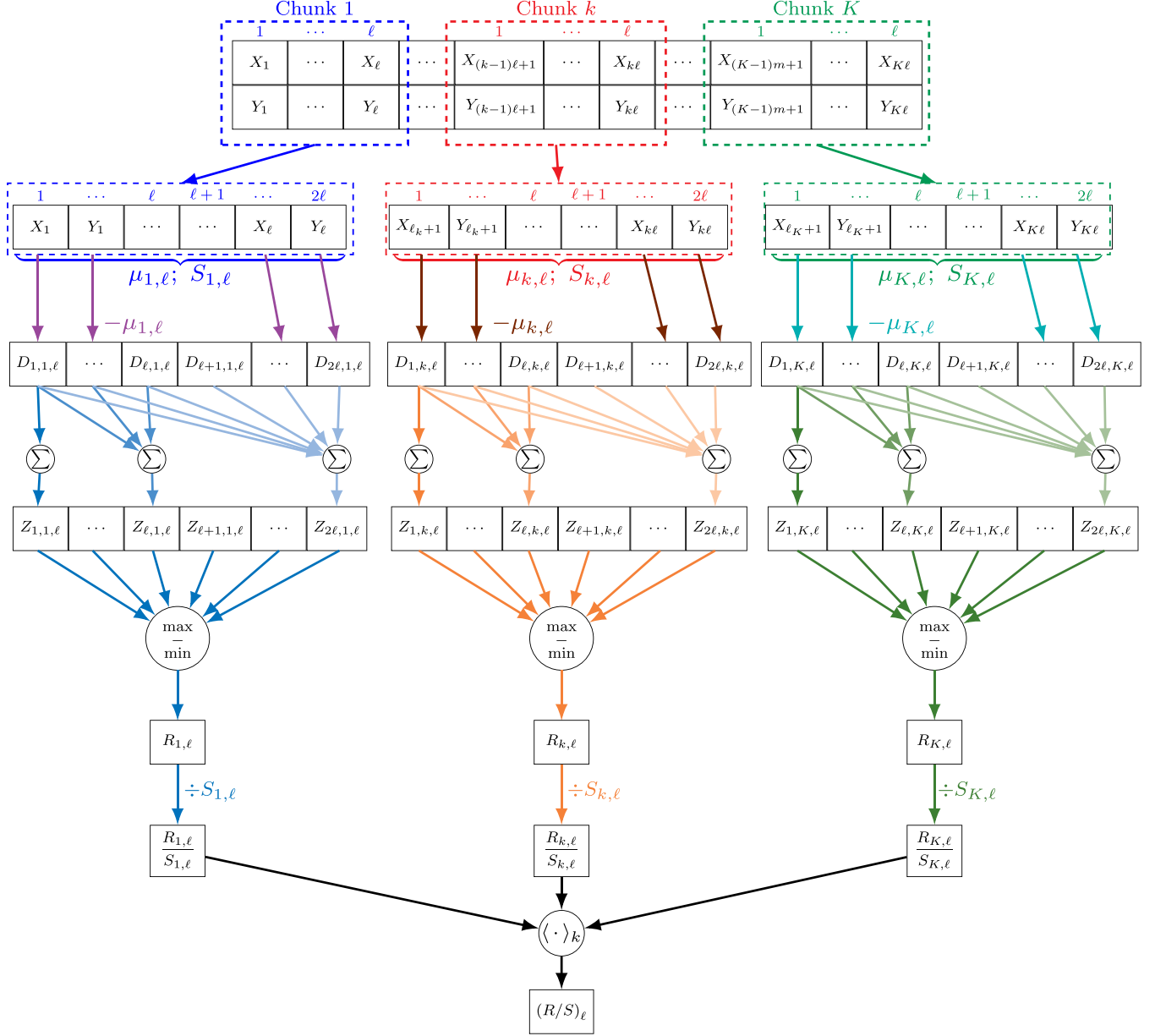


FIG. 9. Scheme evidencing the construction of the partition of a bidimensional time series and the structure of the cumulative sequence for R/S analysis. Note that  $\ell_k := (k-1)\ell$  and  $\ell_K := (K-1)\ell$ .

of  $T = 256$ . Figure 8(b) presents the probability distribution  $P(FTH_{256}(2^{30}))$  for  $\gamma = 0.25$  that reveal a multimodal distribution where the largest maximum corresponding to chaotic sea regions and the different minor peaks are due to the hierarchical islands-around-islands structure embedded in the phase space. Figure 8(c) correlates these multiple peaks with specific regions in the phase space, each represented by a different color. Note that the area in the distribution represented by the green points indicates chaotic orbits that are restricted from accessing specific regions due to the tangency of stable and unstable manifolds [79]. This peak reflects the influence of these manifolds. The yellow regions, on the other hand, represent the chaotic seas that exist among the islands. Additionally, the other smaller peaks correspond to various hierarchical levels around the islands.

## VI. CONCLUSION

Stickiness is a crucial phenomenon in nonlinear dynamics that is difficult to identify in Hamiltonian systems. Various methods for detecting sticky orbits in the phase space of two-dimensional area-preserving systems have been proposed and studied in previous research [18,19,80–82], but these methods typically require a large number of iterations of the map and prior knowledge of the positions of the islands in the phase space. This paper introduces the use of the Hurst exponent to identify and characterize the stickiness effect in the standard map. This method distinguishes between different types of motion in dynamical systems with less complexity than techniques involving recurrence time entropy and Lyapunov exponents, for example. Additionally, it operates based on time

series data, eliminating the requirement for a precisely defined orbit law, which is often unavailable in natural dynamics.

The study reveals insightful relationships between the Lyapunov exponent  $\lambda_{\max}$  and the Hurst exponent  $H$ , as demonstrated in three distinct scenarios [Figs. 3(a) and 3(d), and 3(c) and 3(f)]. This similarity underscores the potential utility and validity of the Hurst exponent in applications traditionally reliant on Lyapunov exponents. Additionally, the study demonstrates that similar conclusions about dynamics can be drawn using the Hurst exponent with smaller time series.

For systems exhibiting the stickiness effect, transitions occur from fully chaotic motion to various levels within the hierarchical structure of islands around islands. When the Hurst exponent was computed in these scenarios, the distribution of finite-time Hurst exponents (FTH) exhibits a multimodal characteristic, with each peak representing a distinct hierarchical level of islands. Furthermore, the robustness of these results is confirmed across different time series lengths and time-window sizes.

Lastly, the methodology was applied to two additional models, the bouncer model and the kicked Harper map, to demonstrate that the Hurst exponent can characterize stickiness in these systems. This extension provides a broader

context for the results and confirms their relevance beyond the Chirikov standard map. The analysis reveals a multimodal distribution, highlighting the presence of dynamical traps, and establishes correlations between the peaks and various structures within the phase space.

## ACKNOWLEDGMENTS

This work was partially supported by FAPESP (No. 2022/03612-6). I would like to acknowledge Matheus Rolim Sales for the valuable discussions.

## APPENDIX: SCHEME OF THE ADAPTED R/S ANALYSIS

The most famous method of estimating the Hurst exponent  $H$  is R/S analysis or range-rescaled analysis. This method involves rescaling the range with the standard deviation. While R/S analysis is typically applied to one-dimensional time series, adaptations are necessary to apply it to bidimensional series, specifically by modifying the construction of the partition. In this Appendix, Fig. 9 presents a scheme of the adapted R/S analysis for a bidimensional time series. To simplify, the notation  $\ell_k := (k - 1)\ell$  and  $\ell_K := (K - 1)\ell$  is used.

- 
- [1] R. Mackay, J. Meiss, and I. Percival, Transport in Hamiltonian systems, *Physica D* **13**, 55 (1984).
  - [2] D. K. Umberger and J. D. Farmer, Fat fractals on the energy surface, *Phys. Rev. Lett.* **55**, 661 (1985).
  - [3] J. D. Meiss and E. Ott, Markov tree model of transport in area-preserving maps, *Physica D* **20**, 387 (1986).
  - [4] A. Alexandre, M. Mangeat, T. Guérin, and D. S. Dean, How stickiness can speed up diffusion in confined systems, *Phys. Rev. Lett.* **128**, 210601 (2022).
  - [5] G. Zaslavsky, Dynamical traps, *Physica D* **168–169**, 292 (2002).
  - [6] V. Afraimovich and G. M. Zaslavsky, Sticky orbits of chaotic Hamiltonian dynamics, in *Chaos, Kinetics and Nonlinear Dynamics in Fluids and Plasmas*, edited by S. Benkadda and G. M. Zaslavsky (Springer, Berlin, Heidelberg, 1998), pp. 59–82.
  - [7] Y. Scher, S. Reuveni, and D. S. Grebenkov, Escape of a sticky particle, *Phys. Rev. Res.* **5**, 043196 (2023).
  - [8] J. D. Meiss, J. R. Cary, C. Grebogi, J. D. Crawford, A. N. Kaufman, and H. D. Abarbanel, Correlations of periodic, area-preserving maps, *Physica D* **6**, 375 (1983).
  - [9] G. Zaslavsky, Chaos, fractional kinetics, and anomalous transport, *Phys. Rep.* **371**, 461 (2002).
  - [10] E. G. Altmann, A. E. Motter, and H. Kantz, Stickiness in mushroom billiards, *Chaos: An Interdiscip. J. Nonlinear Sci.* **15**, 03105 (2005).
  - [11] E. G. Altmann, A. E. Motter, and H. Kantz, Stickiness in Hamiltonian systems: From sharply divided to hierarchical phase space, *Phys. Rev. E* **73**, 026207 (2006).
  - [12] G. Cristadoro and R. Ketzmerick, Universality of algebraic decays in Hamiltonian systems, *Phys. Rev. Lett.* **100**, 184101 (2008).
  - [13] C. F. Karney, Long-time correlations in the stochastic regime, *Physica D* **8**, 360 (1983).
  - [14] B. Chirikov and D. Shepelyansky, Correlation properties of dynamical chaos in Hamiltonian systems, *Physica D* **13**, 395 (1984).
  - [15] C. Efthymiopoulos, G. Contopoulos, N. Voglis, and R. Dvorak, Stickiness and cantori, *J. Phys. A: Math. Gen.* **30**, 8167 (1997).
  - [16] R. S. MacKay, J. D. Meiss, and I. C. Percival, Stochasticity and transport in Hamiltonian systems, *Phys. Rev. Lett.* **52**, 697 (1984).
  - [17] T. Okushima, New method for computing finite-time lyapunov exponents, *Phys. Rev. Lett.* **91**, 254101 (2003).
  - [18] J. D. Szezech, S. Lopes, and R. Viana, Finite-time lyapunov spectrum for chaotic orbits of non-integrable Hamiltonian systems, *Phys. Lett. A* **335**, 394 (2005).
  - [19] M. R. Sales, M. Mugnaine, J. D. Szezech, R. L. Viana, I. L. Caldas, N. Marwan, and J. Kurths, Stickiness and recurrence plots: An entropy-based approach, *Chaos: An Interdiscip. J. Nonlinear Sci.* **33**, 033140 (2023).
  - [20] M. R. Sales, mrolims/StickinessRecurrencePlots: v2.2.0 (v2.2.0), Zenodo (2023), <https://doi.org/10.5281/zenodo.7679173>.
  - [21] L. C. Souza, M. R. Sales, M. Mugnaine, J. D. Szezech, I. L. Caldas, and R. L. Viana, Chaotic escape of impurities and sticky orbits in toroidal plasmas, *Phys. Rev. E* **109**, 015202 (2024).
  - [22] N. B. Slater, The distribution of the integers  $n$  for which  $\theta n < \phi$ , *Math. Proc. Cambridge Philos. Soc.* **46**, 525 (1950).
  - [23] N. B. Slater, Gaps and steps for the sequence  $n\theta \bmod 1$ , *Math. Proc. Cambridge Philos. Soc.* **63**, 1115 (1967).
  - [24] H. E. Hurst, Long-term storage capacity of reservoirs, *Trans. Am. Soc. Civ. Eng.* **116**, 770 (1951).
  - [25] A. Carbone, G. Castelli, and H. Stanley, Time-dependent hurst exponent in financial time series, *Physica A* **344**, 267 (2004).
  - [26] D. Grech and Z. Mazur, Can one make any crash prediction in finance using the local hurst exponent idea?, *Physica A* **336**, 133 (2004).

- [27] M. Couillard and M. Davison, A comment on measuring the hurst exponent of financial time series, *Physica A* **348**, 404 (2005).
- [28] J. A. Matos, S. M. Gama, H. J. Ruskin, A. A. Sharkasi, and M. Crane, Time and scale hurst exponent analysis for financial markets, *Physica A* **387**, 3910 (2008).
- [29] S. Lahmiri, A nonlinear analysis of cardiovascular diseases using multi-scale analysis and generalized hurst exponent, *Healthcare Anal.* **3**, 100142 (2023).
- [30] W.-S. Lam, W. Ray, P. N. Guzdar, and R. Roy, Measurement of hurst exponents for semiconductor laser phase dynamics, *Phys. Rev. Lett.* **94**, 010602 (2005).
- [31] H.-Y. Zhang, Z.-Q. Feng, S.-Y. Feng, and Y. Zhou, Typical algorithms for estimating Hurst exponent of time sequence: A data analyst's perspective, [arXiv:2310.19051](https://arxiv.org/abs/2310.19051).
- [32] C.-K. Peng, S. V. Buldyrev, S. Havlin, M. Simons, H. E. Stanley, and A. L. Goldberger, Mosaic organization of dna nucleotides, *Phys. Rev. E* **49**, 1685 (1994).
- [33] E. Alessio, A. Carbone, G. Castelli, and V. Frappietro, Second-order moving average and scaling of stochastic time series, *Eur. Phys. J. B* **27**, 197 (2002).
- [34] J. Geweke and S. Porter-Hudak, The estimation and application of long memory time series models, *J. Time Ser. Anal.* **4**, 221 (1983).
- [35] B. B. Mandelbrot and J. R. Wallis, Noah, joseph, and operational hydrology, *Water Resour. Res.* **4**, 909 (1968).
- [36] B. B. Mandelbrot and J. R. Wallis, Robustness of the rescaled range r/s in the measurement of noncyclic long run statistical dependence, *Water Resour. Res.* **5**, 967 (1969).
- [37] B. Mandelbrot, *The Fractal Geometry of Nature*, Einaudi paperbacks (W. H. Freeman Company, New York, 1983).
- [38] B. V. Chirikov, A universal instability of many-dimensional oscillator systems, *Phys. Rep.* **52**, 263 (1979).
- [39] J. M. Greene, A method for determining a stochastic transition, *J. Math. Phys.* **20**, 1183 (1979).
- [40] R. MacKay, A renormalization approach to invariant circles in area-preserving maps, *Physica D* **7**, 283 (1983).
- [41] M. R. Sales, M. Mugnaine, R. L. Viana, I. L. Caldas, and J. D. Szezech, Unpredictability in Hamiltonian systems with a hierarchical phase space, *Phys. Lett. A* **431**, 127991 (2022).
- [42] R. M. da Silva, C. Manchein, M. W. Beims, and E. G. Altmann, Characterizing weak chaos using time series of lyapunov exponents, *Phys. Rev. E* **91**, 062907 (2015).
- [43] A. Wolf, J. B. Swift, H. L. Swinney, and J. A. Vastano, Determining lyapunov exponents from a time series, *Physica D* **16**, 285 (1985).
- [44] G. Benettin, L. Galgani, A. Giorgilli, and J. M. Strelcyn, Lyapunov characteristic exponents for smooth dynamical systems and for Hamiltonian systems: A method for computing all of them. part 1: Theory, *Mecchanica* **15**, 9 (1980).
- [45] M. Sano and Y. Sawada, Measurement of the lyapunov spectrum from a chaotic time series, *Phys. Rev. Lett.* **55**, 1082 (1985).
- [46] J. P. Eckmann and D. Ruelle, Ergodic theory of chaos and strange attractors, *Rev. Mod. Phys.* **57**, 617 (1985).
- [47] C. Manchein and M. W. Beims, Conservative generalized bifurcation diagrams, *Phys. Lett. A* **377**, 789 (2013).
- [48] S. Das and J. A. Yorke, Super convergence of ergodic averages for quasiperiodic orbits, *Nonlinearity* **31**, 491 (2018).
- [49] S. Das, C. B. Dock, Y. Saiki, M. Salgado-Flores, E. Sander, J. Wu, and J. A. Yorke, Measuring quasiperiodicity, *Europhys. Lett.* **114**, 40005 (2016).
- [50] M. Harle and U. Feudel, Hierarchy of islands in conservative systems yields multimodal distributions of fles, *Chaos, Solitons Fractals* **31**, 130 (2007).
- [51] T. S. Krüger, P. P. Galuzio, T. d. L. Prado, R. L. Viana, J. D. Szezech, and S. R. Lopes, Mechanism for stickiness suppression during extreme events in Hamiltonian systems, *Phys. Rev. E* **91**, 062903 (2015).
- [52] V. Anishchenko, A. Kopeikin, J. Kurths, T. Vadivasova, and G. Strelkova, Studying hyperbolicity in chaotic systems, *Phys. Lett. A* **270**, 301 (2000).
- [53] T. Kruger, L. D. Pustyl'nikov, and S. E. Troubetzkoy, Acceleration of bouncing balls in external fields, *Nonlinearity* **8**, 397 (1995).
- [54] L. D. Pustyl'nikov, Existence of a set of positive measure of oscillating motions in a certain problem of dynamics, in *Doklady Akademii Nauk*, Vol. 202 (Russian Academy of Sciences, 1972), pp. 287–289.
- [55] L. D. Pustyl'nikov, Stable and oscillating motions in nonautonomous dynamical systems. a generalization of c. l. siegel's theorem to the nonautonomous case, *Math. USSR-Sbornik* **23**, 382 (1974).
- [56] M. Lieberman and V. Godyak, From fermi acceleration to collisionless discharge heating, *IEEE Trans. Plasma Sci.* **26**, 955 (1998).
- [57] A. Lichtenberg, M. Lieberman, and R. Cohen, Fermi acceleration revisited, *Physica D* **1**, 291 (1980).
- [58] A. L. P. Livorati, T. Kroetz, C. P. Dettmann, I. L. Caldas, and E. D. Leonel, Stickiness in a bouncer model: A slowing mechanism for fermi acceleration, *Phys. Rev. E* **86**, 036203 (2012).
- [59] A. L. P. Livorati, D. G. Ladeira, and E. D. Leonel, Scaling investigation of fermi acceleration on a dissipative bouncer model, *Phys. Rev. E* **78**, 056205 (2008).
- [60] E. D. Leonel and A. L. Livorati, Thermodynamics of a bouncer model: A simplified one-dimensional gas, *Commun. Nonlinear Sci. Numer. Simul.* **20**, 159 (2015).
- [61] P. G. Harper, Single band motion of conduction electrons in a uniform magnetic field, *Proc. Phys. Soc. London, Sect. A* **68**, 874 (1955).
- [62] B. Lévi and B. Georgeot, Quantum computation of a complex system: The kicked harper model, *Phys. Rev. E* **70**, 056218 (2004).
- [63] P. Leboeuf, Normal and anomalous diffusion in a deterministic area-preserving map, *Physica D* **116**, 8 (1998).
- [64] P. Leboeuf, J. Kurchan, M. Feingold, and D. P. Arovas, Phase-space localization: Topological aspects of quantum chaos, *Phys. Rev. Lett.* **65**, 3076 (1990).
- [65] R. Lima and D. Shepelyansky, Fast delocalization in a model of quantum kicked rotator, *Phys. Rev. Lett.* **67**, 1377 (1991).
- [66] U. Tirnakli, C. Tsallis, and K. Cetin, Dynamical robustness of discrete conservative systems: Harper and generalized standard maps, *J. Stat. Mech.: Theory Exp.* (2020) 063206.
- [67] S. Shinohara, The threshold for global diffusion in the kicked harper map, *Phys. Lett. A* **298**, 330 (2002).
- [68] G. M. Zaslavsky, Stochastic webs and their applications, *Chaos: An Interdiscip. J. Nonlinear Sci.* **1**, 1 (1991).
- [69] G. M. Zaslavsky, *The Physics of Chaos in Hamiltonian Systems*, 2nd ed. (Imperial college press, London, 2007).

- [70] A. J. Lichtenberg and B. P. Wood, Diffusion on two space and time scales, *Phys. Rev. Lett.* **62**, 2213 (1989).
- [71] G. Park and C. S. Chang, Diffusion by extrinsic noise in the kicked harper map, *Phys. Rev. E* **63**, 066213 (2001).
- [72] G. Zaslavskii, M. I. Zakharov, A. Neishtadt, R. Sagdeev, and D. Usikov, Multidimensional Hamiltonian chaos, *Zh. Eksp. Teor. Fiz.* **96**, 1563 (1989).
- [73] A. J. Lichtenberg and B. P. Wood, Diffusion through a stochastic web, *Phys. Rev. A* **39**, 2153 (1989).
- [74] C. F. F. Karney, Stochastic ion heating by a lower hybrid wave: II, *Phys. Fluids A* **22**, 2188 (1979).
- [75] I. Dana, Kicked harper models and kicked charge in a magnetic field, *Phys. Lett. A* **197**, 413 (1995).
- [76] P. Leboeuf, J. Kurchan, M. Feingold, and D. P. Arovas, Topological aspects of quantum chaos, *Chaos: An Interdiscip. J. Nonlinear Sci.* **2**, 125 (1992).
- [77] G. Zaslavskii, R. Sagdeev, and A. Chernikov, Stochastic nature of streamlines in steady-state flows, *Zh. Eksp. Teor. Fiz.* **94**, 102 (1988).
- [78] R. A. Pasmanter, From chaotic advection to chaotic schrödinger-type equations, *Phys. Rev. A* **42**, 3622 (1990).
- [79] J. D. Szezech, A. Schelin, I. Caldas, S. Lopes, P. Morrison, and R. Viana, Finite-time rotation number: A fast indicator for chaotic dynamical structures, *Phys. Lett. A* **377**, 452 (2013).
- [80] M. S. Santos, M. Mugnaine, J. D. Szezech, A. M. Batista, I. L. Caldas, and R. L. Viana, Using rotation number to detect sticky orbits in Hamiltonian systems, *Chaos: An Interdiscip. J. Nonlinear Sci.* **29**, 043125 (2019).
- [81] Y. Zou, M. Thiel, M. C. Romano, and J. Kurths, Characterization of stickiness by means of recurrence, *Chaos: An Interdiscip. J. Nonlinear Sci.* **17**, 043101 (2007).
- [82] C. V. Abud and R. E. de Carvalho, Multifractality, stickiness, and recurrence-time statistics, *Phys. Rev. E* **88**, 042922 (2013).